Measurement of Microscopic Thermal Diffusivity Distribution for Ryugu Sample by Infrared Lock-in Periodic Heating Method

Takuya Ishizaki[1], Hosei Nagano[2], Satoshi Tanaka[1], Naoya Sakatani[1], Tomoki Nakamura[3], Tatsuaki Okada[1], Ryohei Fujita[2], Abdulkareem Alasli[2], Tomoyo Morita[3], Mizuha Kikuiri[3], Kana Amano[3], Eiichi Kagawa[3], Hisayoshi Yurimoto[4], Takaaki Noguchi[5], Ryuji Okazaki[6], Hikaru Yabuta[7], Hiroshi Naraoka[6], Kanako Sakamoto[1], Shogo Tachibana[8, 1], Sei-ichiro Watanabe[2], Yuichi Tsuda[1]

[1]Japan Aerospace Exploration Agency, 3-1-1 Yoshinodai, Sagamihara, Kanagawa 252-5210, Japan
[2]Nagoya University, Furo-cho, Chikusa-ku, Nagoya, Aichi 464-8603, Japan
[3] Tohoku University, Aramaki, Aoba-ku, Sendai, Miyagi 980-8578, Japan
[4] Hokkaido University, 5, Kitahachijonishi, Kita-ku, Sapporo, Hokkaido 060-0810, Japan
[5] Kyoto University, Yoshidahonmachi, Sakyo-ku, Kyoto, Kyoto 060-0810, Japan
[6] Kyushu University, 744 Motooka, Nishi-ku, Fukuoka 819-0395, Japan
[7] Hiroshima University, 1-3-2 Kagamiyama, Higashihiroshima, Hiroshima 739-8526, Japan
[8] The University of Tokyo, 7-3-1 Hongo, Bunkyo-ku, Tokyo 113-0033, Japan

Abstract

The thermophysical properties of small Solar System bodies are essential to be determined, on which the thermal evolution of small bodies largely depends. The carbonaceous asteroid Ryugu is one of the small undifferentiated bodies formed in the early Solar System. Hayabusa2 explored the asteroid Ryugu and returned the surface samples in 2020 for detailed on-ground investigation, including measurements of thermal properties. Because the available sample amount was limited, this study developed a novel method to measure the thermal diffusivity of small and irregularly shaped samples of about 1 mm in diameter by combining lock-in thermography and periodic heating methods on the microscale. This method enables us to measure the thermal diffusivity of both flat-plate and granular shape samples by selecting the suitable detecting direction of the temperature response. Especially, when the sample has a flat-plate shape, the anisotropic distribution of the in-plane thermal diffusivity can be evaluated. This method was applied to six Ryugu samples, and the detailed anisotropic distribution of the thermal diffusivity was obtained. The measurement results showed that the samples show local thermal anisotropy caused by cracks and voids. The average thermal diffusivity among all samples was $(2.8-5.8) \times 10^{-7}$ m^2/s. Based on the density and specific heat of the samples obtained independently, the thermal effusivity was estimated to be 791−1253 $J/(s^{1/2}m^2K)$, which is defined as the resistance of surface temperature to the change of thermal input. The determined thermal effusivity, often called thermal inertia in planetary science, is larger than the observed value of 225 ± 45 $J/(s^{1/2}m^2K)$ of the asteroid Ryugu's surface, obtained from the diurnal temperature change of the rotating asteroid by a thermal infrared camera onboard Hayabuas2. This difference is likely to be attributed to the difference in the analytical scale between the sample and the surface boulders compared with the thermal diffusion length. Consequently, it was found that the present result is more representative of the thermal diffusivity and thermal inertia of local part of individual Ryugu particles.

Keywords: Asteroid; Distribution; Measurement method; Microscale; Non-contact; Ryugu; Thermal diffusivity; Thermal

effusivity; Thermal inertia

1 Introduction

The Solar System bodies formed and evolved over a long period of time through repeated collision, fragmentation, and accretion of planetesimals formed in the early Solar System. However, their evolution mechanism of when and under what conditions accretion and collisions will form today's planets and asteroids has not yet been clarified. Carbonaceous (C-type) asteroids have been considered primitive bodies that record their formation history in the early Solar System. Therefore, C-type asteroids are expected to provide important clues to elucidate the formation and evolution of the Solar System's small bodies. Hayabusa2 explored the C-type near-Earth asteroid Ryugu and brought back a ~5 g sample in 2020. The chemical analysis of the returned sample shows that Ryugu consists of materials similar to a primitive Ivuna-type carbonaceous chondrite（CI chondrite) [1], which is the closest to the average composition of the Solar System among the carbonaceous chondrites. Additionally, chemical analysis, which includes light element such as C, N, and O, of a large amount Ryugu samples more than 100 mg using muon also revealed that Ryugu has a composition similar to CI chondrite [2].

C-type asteroids are abundant in the outer asteroid main belt [3–5], and Ryugu, which has a rubble pile structure formed by the reassembly of fragments of its parent asteroid [6], is thought to have originated there. It has been proposed that the asteroid changed its orbit from the outer main belt to the orbits of the Eulalia or Polana C families in the inner asteroid main belt, which are considered to be its direct origin [7–10], and then to the current Earth-crossing orbit. In order to understand the size, formation timing, and thermal and collisional history of CI-like Ryugu's planetesimal in the early Solar System, the formation of the current Ryugu as a rubble pile body, and its orbital evolution to the near-Earth orbit, it is of importance to determine thermophysical properties of Ryugu materials, such as thermal conductivity, to be included in thermal, physical, and orbital evolution models.

For a long time, thermophysical properties used in models of the thermal evolution of hydrated asteroids and icy bodies have been assumed to be those of serpentine, which is a hydrous mineral abundant in carbonaceous chondrites [11–13]. The thermal conductivity of serpentine is smaller than those of other rocky materials [10]. Opeil et al. [10] reported that the thermal conductivity of Mighei-type carbonaceous chondrites (CM chondrites) is even smaller than that of serpentine, less than one-fourth [11]. Although no thermal conductivity data have been reported for CI chondrites, which are taxonomically closer to Ryugu, they are thought to have even lower thermal conductivity because of their smaller bulk density and higher porosity than other carbonaceous chondrites [14]. Therefore, previous thermal evolution models may have used higher thermal conductivities to apply the thermal evolution of CI planetesimals. Therefore, measuring the thermal conductivity of returned samples is extremely important to determine the thermal conductivity to construct the thermal evolution model for Ryugu.

Although several measurements of thermal conductivity or thermal diffusivity of chondrites have been reported [15,16], the methods used for these measurements required contact with the sample and shape processing of the sample, these methods are not acceptable for Ryugu samples because of their limited amounts and size. Furthermore, it has been known that the thermal conductivity of chondrites differ among samples even if with the same taxonomic class, and these differences are thought to be due to differences in density, porosity, crack distribution, and texture, which leads to an anisotropic effect [17]. Therefore, to determine the thermal conductivity, it is desirable to evaluate its anisotropy through

statistical measurements rather than determining a representative sample value via measurement along only one direction. To satisfy this requirement, in this work, a non-contact thermal diffusivity distribution measurement method for small particles by a periodic heating method using lock-in thermography (LIT) was developed [16].

In the initial analysis of the Ryugu sample, seventeen individual particles were allocated for evaluation out of the returned sample of more than 1,700 particles (total amount of 5.4 g). The thermal diffusivity measurement was one of the initial analysis items. Thermal diffusivity distributions were evaluated for five of them using the developed measurement method. the total number of samples used in this study is six because one of the particles was sliced into two pieces. Based on the thermophysical property determined for one of the samples (C0002), a thermal evolution model calculation of Ryugu was performed, which supports theoretical predictions of the formation period, location, size, water-rock mass ratio, and temperature history of the Ryugu precursor [2]. In this paper, all thermal diffusivity measurements made in the initial analysis are reported in detail. Additionally, the density and specific heat were converted to thermal effusivity. Since effective thermal effusivity is called "thermal inertia" in the planetary science field, effective thermal effusivity will be referred as thermal inertia in this paper.

2 Measurement Principle

In the periodic heating method, the sample surface is modulated by a laser spot, and the thermal diffusivity in the sample cross-section direction is measured from the temperature response detected on the rear surface by lock-in thermography. When there is a periodic point heat source of $\dot{Q}\mathrm{e}^{i(2\pi ft)}$ on the surface of a continuous medium, the AC temperature $T_{ac}(r,t)$ at a distance r and a time t is expressed by Equation (1) [18],

$$T_{ac}(r,t) = \frac{\dot{Q}}{4\pi\lambda r}\exp\{(-kr + i(2\pi ft - kr)\}, \tag{1}$$

where $\dot{Q}$ is the heat input, λ is the thermal conductivity, f is the heating frequency, and k is the wavenumber, which is expressed as

$$k = \sqrt{\frac{\pi f}{D}}, \tag{2}$$

where D is the thermal diffusivity. From Equation (1), the phase delay θ at distance r from the periodic point heat source is,

$$\theta = kr = \sqrt{\frac{\pi f}{D}}r \tag{3}$$

and by differentiating Equation (3) by distance r, the thermal diffusivity D can be expressed by Equation (4),

$$D = \frac{\pi f}{(d\theta/dr)^2} \tag{4}$$

Equation (1) is based on infinite body despite sample's complicated boundary. Then sample is approximated to infinite media by selecting the appropriate heating frequency at which the reflected temperature wave from the sample boundary does not affect to the result. As Equation (1) is the AC temperature component of the temperature response, it indicates that the AC temperature is more attenuated when heating frequency becomes higher. In the actual measurement, the heating frequency is selected to avoid the influence of the reflected temperature wave by trying measurements with some frequencies [19,20]. Also, Equation (1) is based on isotropic thermophysical properties despite sample's anisotropic ones. The validity of this simplification is proven by Mendioroz et al. [21] that even if a material has anisotropic thermophysical properties, the phase lag has a linear dependence on the distance with the slope defined by the thermal diffusivity of the only its direction.

3 Measurement Apparatus

The schematic of the measurement apparatus is shown in Figure 1. This apparatus consisted of a function generator, lock-in thermography device with an infrared microscope, diode laser, beam expander, objective lens, complementary metal-oxide-semiconductor (CMOS) camera, sample, vacuum chamber, and computer. The function generator oscillated the modulation signal to the diode laser and lock-in thermography. The diode laser then emitted the modulated beam according to the modulation signal. The beam was focused onto the sample's surface through the objective lens with monitoring by a CMOS camera. The minimum laser spot diameter is estimated to be about 7 μm. The wavelength of the diode laser was 638 ± 5 nm, and the maximum output power of the continuous wave was 150 mW. Although the temperature resolution of LIT is 30 mK, the detectable amplitude can be enhanced to less than 1 mK by lock-in analysis. The camera's spatial resolution can be selected from 1.6, 2.5, and 5.1 μm depending on the apparatuses (three apparatuses are available). However, the spatial resolution of temperature detection is limited to the diffraction limit of 1.7−3.6 μm because of Rayleigh's diffraction limit. The diffraction limit is decided by a numerical aperture and the detection wavelength range of LIT is 2.5−5.1 μm using InSb photodetectors. The measurement results have no dependence on apparatuses because the analysis region is larger enough than the spatial resolution of LIT. The pressure in the vacuum chamber is on the order of 10^{-3} Pa.

The heating surface and the detecting surface are changed according to the sample shape by changing the sample holder, as shown on the right side of Figure 2. When the sample has a thin-plate-like shape, the thermal response is measured from the front side while the rear surface is periodically heated (Figure 2 (a)). This enables us to obtain the full-angle distribution of the in-plane thermal diffusivity centered on the heating point. On the other hand, when the sample has a granular shape, selecting a horizontal flat surface for detection and a vertical flat surface for heating by aligning the laser beam horizontally (Figure 2 (b)). In this case, the heating point is placed to coincide with the edge of the sample. In this way, the semicircle distribution of the thermal diffusivity around the heating point can be obtained.

The uncertainty β of the measurement method was estimated by the following formula [19],

$$\beta = 2\sqrt{\frac{D}{\pi f}}|\Delta S|. \tag{5}$$

where, ΔS is the standard error of the slope of the phase lag $d\theta/dr$, and it is estimated by dividing the standard error of phase lag by distance r. Here, the standard error of the phase lag was defined by the double standard deviation of the detrended phase lag. In the measurements conducted here, ΔS was simultaneously analyzed with the thermal diffusivity in each direction. Then, the error range of $\beta \cdot D$ was expressed as an error bar in the figure.

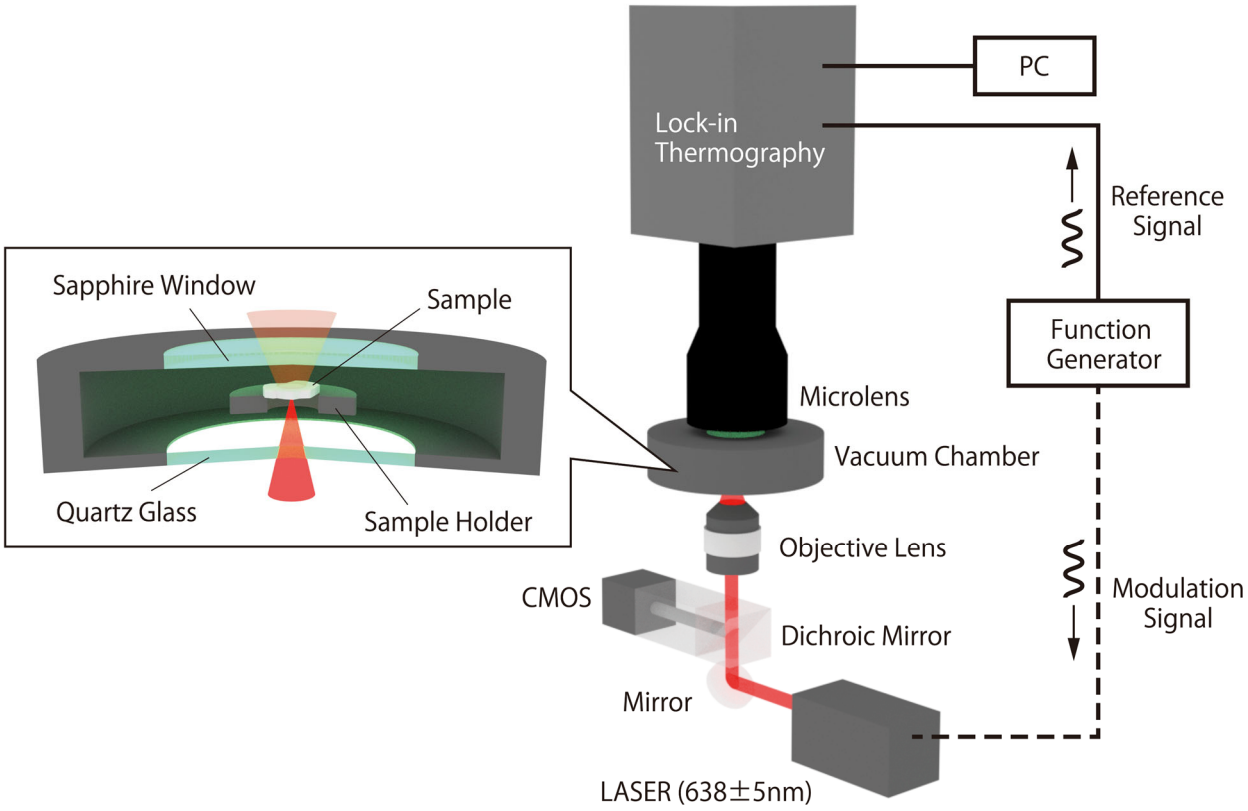

Figure 1 Schematic of Measurement apparatus.

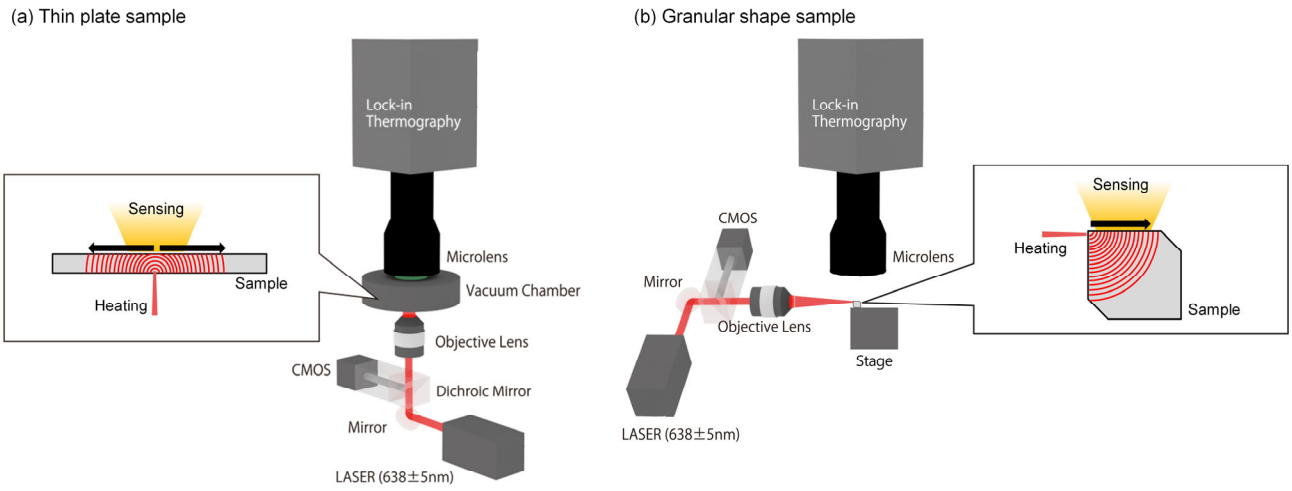

Figure 2 Measurement sample configuration; (a) for thin plate sample, (b) for granular shape sample.

4 Samples and Measurement Condition

Six Ryugu samples were analyzed; C0002-plate 3 (C0002-p3), C0002-plate 4 (C0002-p4), C0025, A0026, C0033, and A0064. A0026 and A0064 are the particles collected at the first touchdown site, and C0002, C0025, and C0033 from the second touchdown site [22,23]. C0002-p3 and C0002-p4 were plate-shaped samples cut out from the grain C0002, which is the third largest sample among all the returned particles. Optical microscopic images of samples are shown in Figure 3, and the sample sizes, bulk densities [2] and the surfaces selected to be heated are summarized in Table 1. Only C0002-p3 and C0002-p4 were measured by the rear-heating method due to their thin plate shapes. In Figure 3, the red point indicates the heated point, and the dashed line indicates the lock-in thermography's field of view (FOV). In the photo of C0002-p3, areas of different compositions or defects can be identified as some dark region in the upper left of the heating point. Then, C0025 has a partially cracked appearance, while A0026 has fewer cracks and a shiny appearance. C0033 is similar to C0025 in appearance but has a larger bulk density. Therefore, C0033 possibly has fewer voids and cracks inside the body. It was harder to select the heating and detection surface for A0064 due to its roundish shape with an aspect ratio of ~1.

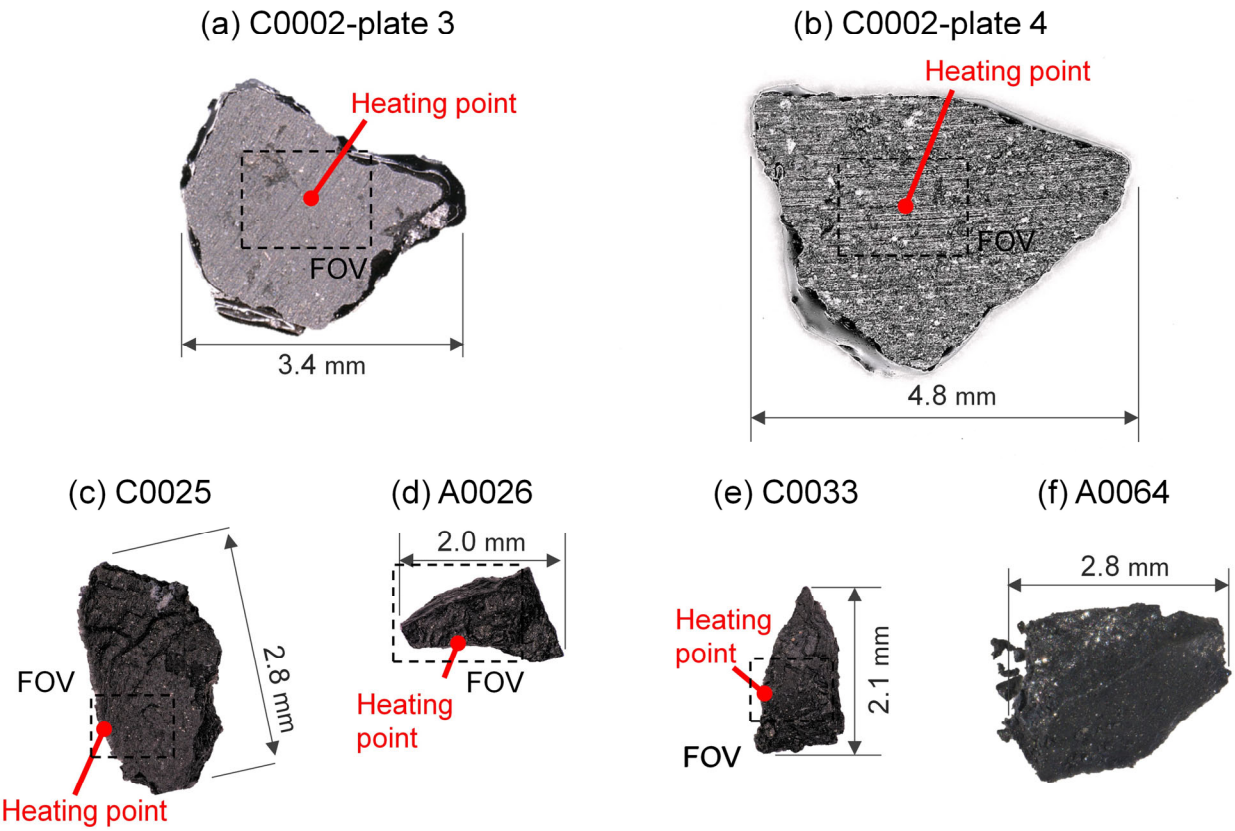

Figure 3 Optical microscopic images of measured samples; (a) C0002-plate 3, (b) C0002-plate 4, (c) C0025, (d) A0026, (e) C0033, and (f) A0064.

Table 1 Sample specification and measurement method.

Sample	C0002-p3	C0002-p4	C0025	A0026	C0033	A0064
Shape	Thin plate	Thin plate	Granular	Granular	Granular	Granular
Size, mm	3.4 × t0.77	4.8 × t0.93	2.8	2.0	2.1	2.8
Density [2], kg/m^3	1820 ± 49	1820 ± 49	1790 ± 20	1650 ± 78	1920 ± 13	1860 ± 15
Heating	Rear	Rear	Side	Side	Side	Side

Table 2 lists the measurement conditions of thermal diffusivity. The laser output power of the C0002-p3 and p4 samples was set to be larger than other samples. This is because the farer detection surface from the heating point of these samples affects the temperature attenuation within the samples. The heating frequency was selected according to the sample size so that the temperature response of the sensing surface was not affected by temperature waves reflected at the sample boundary. The higher the heating frequency, the smaller the effect of reflected waves, but the noise level of the detected signal also increases. Because of its round shape, A0064 has a less flat area and is more susceptible to reflected waves, and measurements were taken at the highest frequencies. C0002-p3 and A0064 were measured under vacuum pressure, and C0025, A0026, and C0033 were measured under atmospheric pressure ("Ambient" in Table 2). C0002-p4 was measured

under both vacuum and atmospheric pressure to assess the influence of air. The differences in spatial resolution of the measured samples are due to utilizing different measurement apparatuses, as discussed in section 3. All measurements were conducted at room temperature (RT).

Table 2 Measurement conditions.

Sample	C0002-p3	C0002-p4	C0025	A0026	C0033	A0064
Laser output power	20 mW	20 mW	10 mW	10 mW	10 mW	10 mW
Heating freq.	2.0 Hz	1.0 Hz	4.0 Hz	4.0 Hz	4.0 Hz	20.0 Hz
Pressure	Vacuum	Vacuum and Ambient	Ambient	Ambient	Ambient	Vacuum
Spatial resolution	2.5 μm	2.5 μm	1.6 μm	2.5 μm	1.6 μm	5.1 μm
Temperature	RT	RT	RT	RT	RT	RT

5 Results and Discussion

5.1 Thermal diffusivity of Ryugu samples

Figures 4-9 show the optical microscope images, corresponding phase lag distribution maps, and thermal diffusivity distribution analysis results for each sample. Analytical uncertainties indicated by error bars in the thermal diffusivity distribution were calculated using Equation (5). The optical microscope image of Figure 4(a) shows that C0002-plate 3 has a dark region that may have different physical and/or chemical properties from other regions on the upper-left of the heating point, and the phase lag map shows that the phase lag in the corresponding region increases (Figure 4(b)). The increase of the phase lag results in the decrease of the thermal diffusivity in the direction between 120 degrees and 180 degrees (Figure 4(c)). Such low thermal diffusivity indicates the presence of materials with low thermal diffusivity or structural defects such as cracks. The maximum and minimum values of thermal diffusivity are 7.6×10^{-7} and 2.0×10^{-8} m^2/s, and the average value of $(2.8 \pm 0.7) \times 10^{-7}$ m^2/s was obtained. The Ryugu sample is not a homogeneous material consisting of a single substance, but a composite of several minerals. And the size of some large mineral grains is about several tens of microns, as can be seen in the microscope image. Since the laser spot size is about 7 μm, the thermal diffusivity distributions obtained by this method will differ depending on the positional relationship between heating point and mineral composition on sample surface. In other words, the measurement results in this paper are not representative of the entire sample, but they represent the thermal diffusivity of a radial area with its thermal diffusion length centered on the heating point.

C0002-plate 4 does not seem to have cracks in its appearance (Figure 5(a)), but the thermal diffusivity measured under vacuum conditions showed that the thermal diffusivity varied greatly depending on the direction (Figure 5(c)). The distribution of thermal diffusivity obtained in this method should reflect the heterogeneous distribution of materials and/or structures preventing thermal conduction within the sample. Additionally, the anisotropy of thermal diffusivity is larger and the thermal diffusivity is smaller under vacuum than in the air. The factor preventing thermal conduction, therefore, should be voids or cracks. The maximum and minimum thermal diffusivities under vacuum conditions were 1.1×10^{-6} m^2/s and 7.0×10^{-8} m^2/s, respectively, with an average value of $(3.3 \pm 0.8) \times 10^{-7}$ m^2/s. The maximum value under atmospheric pressure was 6.0×10^{-7} m^2/s, the minimum value was 3.1×10^{-7} m^2/s, and the mean value was $(4.5 \pm 1.2) \times 10^{-7}$ m^2/s. The thermal diffusivity of C0002 reported by Nakamura et al. of $(3.2 \pm 0.3) \times 10^{-7}$ m^2/s [2] was obtained from

the average of the diffusivities measured for C0002-plate 3 and C0002-plate 4 in this study and measured for C0002-plate 4 in National Institute of Advanced Industrial Science and Technology in Japan, which is consistent with our results within a measurement uncertainty.

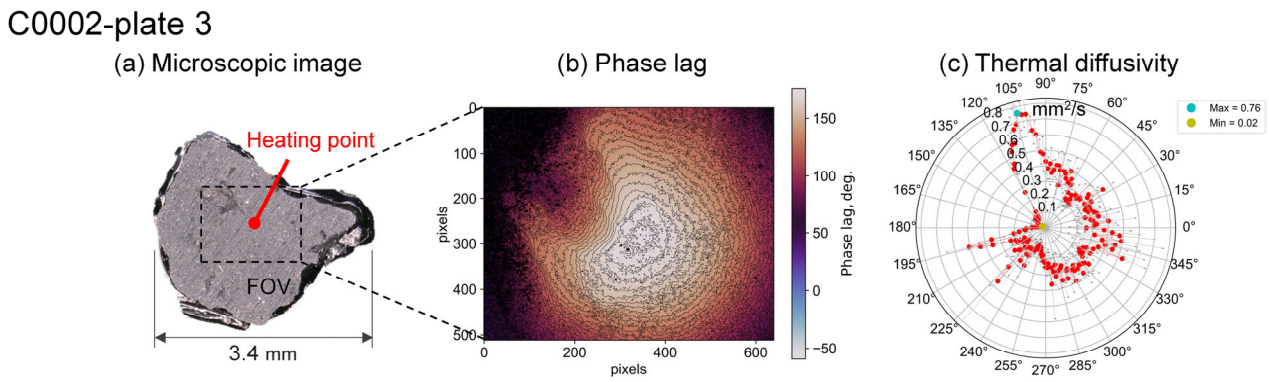

Figure 4 (a) Optical microscopic image, (b) phase lag distribution and (c) thermal diffusivity distribution of C0002-plate 3 sample.

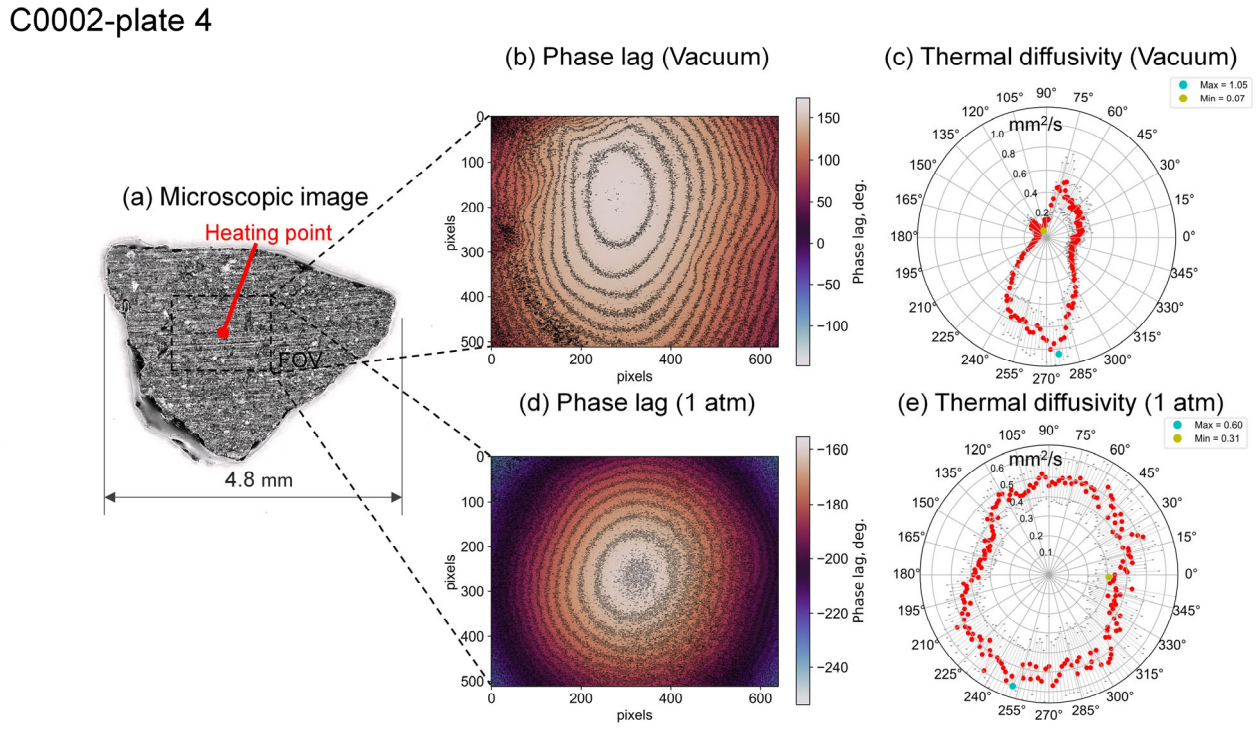

Figure 5 (a) Optical microscopic image, (b) phase lag distribution under vacuum pressure, (c) thermal diffusivity distribution under vacuum pressure, (d) phase lag distribution under atmospheric pressure, and (e) thermal diffusivity distribution under atmospheric pressure of C0002-plate 4 sample. The maximum value of 1.05 mm^2/s is round off to one decimal place in the manuscript.

C0025 (Figure 6) seems to have many cracks from its microscopic image, and cracks are expected to exist parallel to the

sample edge in the vicinity of the heating point placed at the edge of the sample, which prevents thermal diffusion perpendicular to the edge. That results in an anisotropic thermal diffusivity distribution spreading along the edge. The maximum thermal diffusivity was 1.1×10^{-6} m^2/s, the minimum was 3.6×10^{-7} m^2/s, and the average was $(5.6 \pm 1.0) \times 10^{-7}$ m^2/s. In contrast, the thermal diffusivity distribution of A0026 (Figure 7) is isotropic, as indicated by the appearance showing few cracks. The maximum and minimum thermal diffusivities were 6.0×10^{-7} and 3.5×10^{-7} m^2/s, respectively, with an average of $(5.1 \pm 0.2) \times 10^{-7}$ m^2/s. The variation of measured values and the uncertainty of the diffusivity along one direction were the smallest, suggesting that cracks affect not only the anisotropy but also the variation of the thermal diffusivity. The thermal diffusivity distribution of C0033 (Figure 8), which has a similar appearance to that of C0025, shows a large scatter and a large anisotropy. The maximum value of the thermal diffusivity of C0033 is 8.2×10^{-7} m^2/s, and the minimum value is 2.7×10^{-7} m^2/s. The average value is $(5.8 \pm 1.1) \times 10^{-7}$ m^2/s. C0025, A0026, and C0033 were only measured at atmospheric pressure because they were measured before the vacuum chamber was completed.

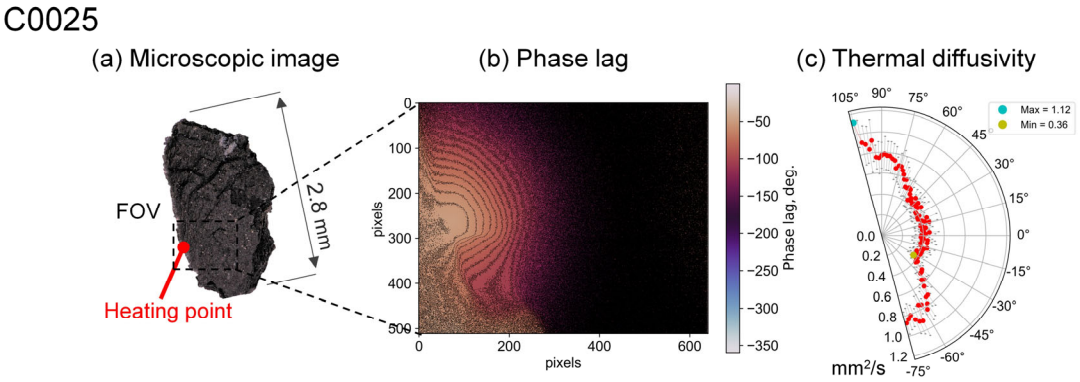

Figure 6 (a) Optical microscopic image, (b) phase lag distribution, and (c) thermal diffusivity distribution of C0025 sample. The maximum value of 1.12 mm^2/s is round off to one decimal place in the manuscript.

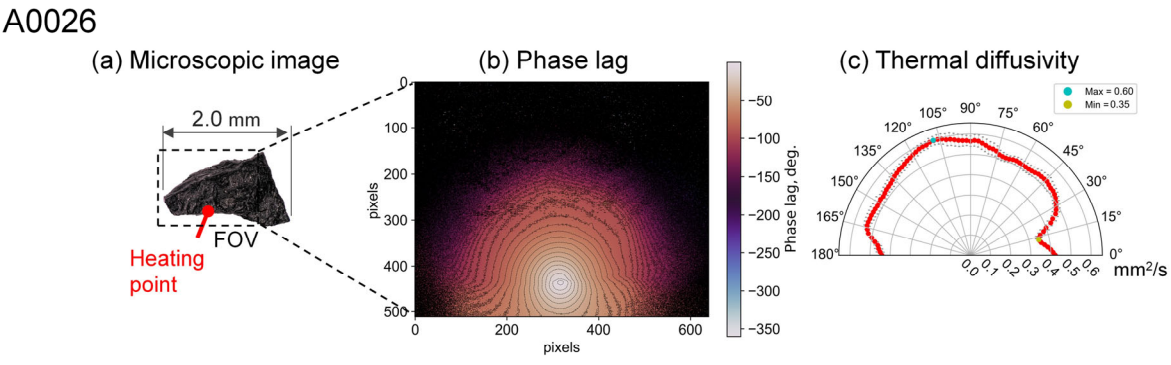

Figure 7 (a) Optical microscopic image, (b) phase lag distribution, and (c) thermal diffusivity distribution of A0026 sample.

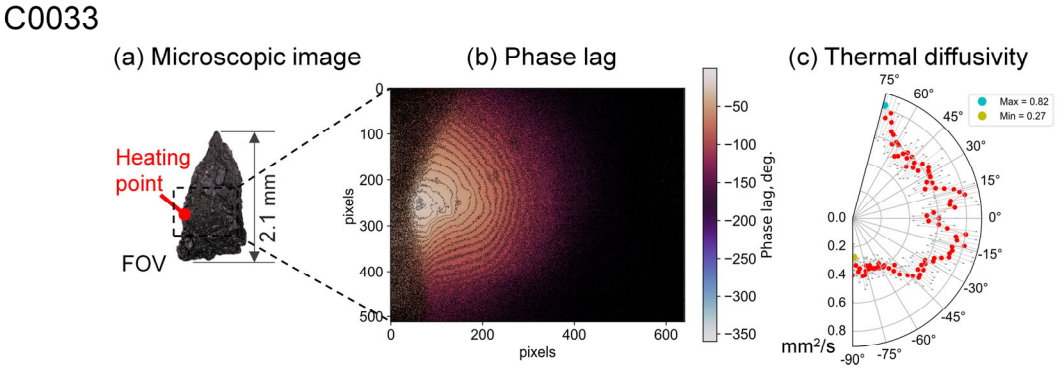

Figure 8 (a) Optical microscopic image, (b) phase lag distribution, and (c) thermal diffusivity distribution of C0033 sample.

The thermal diffusivity distribution of A0064 (Figure 9) is nearly isotropic with a small variation similar to that of A0026 (Figure 7). Therefore, A0064 is likely to have few cracks contributing to anisotropy at this measurement scale, like A0026. The maximum and minimum thermal diffusivities of A0064 were 4.5×10^{-7} and 2.5×10^{-7} m^2/s, respectively, with an average of $(3.3 \pm 0.3) \times 10^{-7}$ m^2/s. The average thermal diffusivity of A0064 is about 35% smaller than that of A0026. This difference may be attributed to the measurement condition; A0064 was measured under vacuum conditions, while A0026 was measured in air. The air filled in the micro or nano voids may have enhanced heat conduction of the sample, resulting in a larger thermal diffusivity of A0026 than that of A0064 measured under vacuum conditions. If this is the case, A0026 and A0064 with a similar thermal isotropy due to fewer cracks may have difference in the measured thermal diffusivity implying that voids are relatively homogeneously distributed in Ryugu samples on much smaller scale than the measurement scale. In order to verify this possibility, future statistical work is necessary for more Ryugu particles with a detailed investigation of internal structures. Non-destructive X-ray computed tomography would be the best way to be combined with thermophysical measurements.

All the data from the six samples are summarized in Table 3. As described above, the maximum and minimum values of thermal diffusivities show a large variation among the samples, and some grains show a large anisotropy. The averaged diffusivity, however, shows a smaller variation. Considering that a larger value tends to be obtained in the air than under vacuum, the averaged thermal diffusivity of six grains would be (3–4) $\times 10^{-7}$ m^2/s.

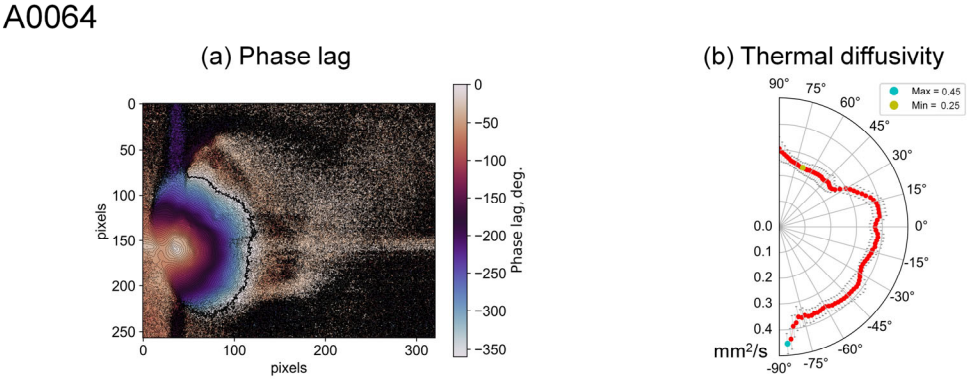

Figure 9 (a) phase lag distribution and (b) thermal diffusivity distribution of the A0064 sample.

Table 3 Summary of thermal diffusivity measurements of Ryugu samples.

Sample	C0002-p3	C0002-p4	C0025	A0026	C0033	A0064
Pressure	Vacuum	Vacuum & Ambient	Ambient	Ambient	Ambient	Vacuum
Max., $\times 10^{-7}$ m^2/s	7.5	10.5 (Vac.) 6.0 (Amb.)	11.2	6.0	8.2	4.5
Avg., $\times 10^{-7}$ m^2/s	2.8 ± 0.7	3.3 ± 0.8 (Vac.) 4.5 ± 1.2 (Amb.)	5.6 ± 1.0	5.1 ± 0.2	5.8 ± 1.1	3.3 ± 0.3
Min., $\times 10^{-7}$ m^2/s	0.2	0.7 (Vac.) 3.1 (Amb.)	3.6	3.4	2.7	2.5
Max./Min.	37.5	15.0 (Vac.) 1.94 (Amb.)	3.11	1.76	3.04	1.80

5.2 Thermal conductivity and thermal inertia of Ryugu samples

Figure 10 compares the thermal conductivities and thermal inertia of six Ryugu grains, converted from the measured thermal diffusivities (Table 3) using grain densities (Table 1) and the specific heat of 865 ± 16 J/(kg·K) (213−373 K for C0002 and A0026) [2] with those of serpentinite. The thermal inertia of the Ryugu surface boulders obtained by the thermal infrared camera onboard Hayabusa2 [5,24] is also compared. Error bars in the figure represent the range between maximum and minimum values. The obtained thermal conductivity and thermal inertia for each sample are summarized in Table 4 and Table 5, respectively.

The results indicate that the thermal conductivity of Ryugu is on average about 73% smaller than that of serpentine (2.5 W/(m·K) [11]). As mentioned above, the thermal conductivity of serpentine has been used in calculations of thermal evolution models for carbonaceous asteroids and comets, and thus may influence the predictions of celestial body sizes and thermal history in small body formation models.

Comparison of the thermal inertia with that observed by Hayabusa2 revealed that the thermal inertia of the Ryugu sample is on average about 3.5 times larger than that of the surface of the asteroid Ryugu (225 ± 45 J/(s$^{1/2}$m^{2}K) [5,24]) except for the minimum value obtained for C0002-p3. Consistency with observed values at minimum value suggests that the value of thermal effusivity varies depending on the measurement scale. In the present measurement, the thermal diffusivity was evaluated in the region of several hundreds of micrometers as thermal diffusion length, whereas the Hayabusa2 observations were made at depths down to several centimeters (thermal skin depth) because the thermal inertia was analyzed using the diurnal variation of the surface temperature due to the 7.6-hour rotation period of asteroid Ryugu. Therefore, it is possible that large-scale cracks caused by meteor impacts and thermal stresses on a scale larger than several hundreds of micrometers are widely developed in rocks and boulders on Ryugu.

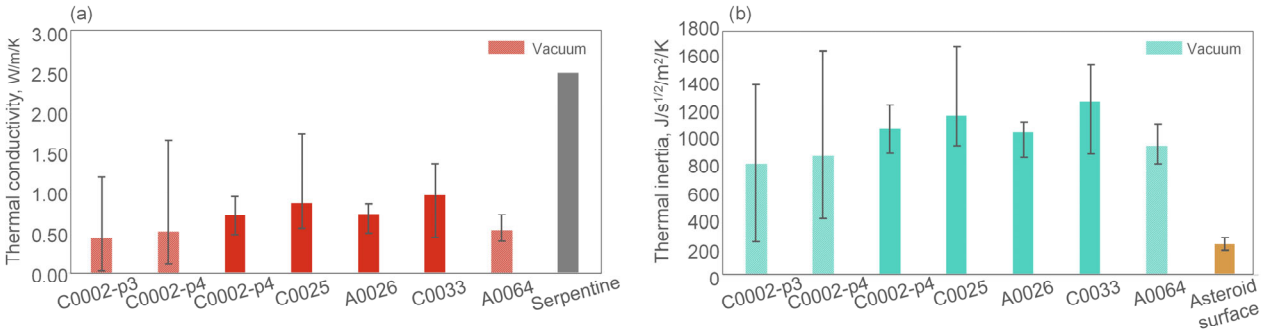

Figure 10 (a) Comparison of the average thermal conductivity of Ryugu samples and serpentine [11], and (b) Comparison of the average thermal inertia of Ryugu samples and the thermal inertia of the asteroid surface of Ryugu observed using the thermal infrared camera on Hayabusa2 [5,24].

Table 4 Summary of calculated thermal conductivity of Ryugu samples.

Sample	C0002-p3	C0002-p4	C0025	A0026	C0033	A0064
Pressure	Vacuum	Vacuum & Ambient	Ambient	Ambient	Ambient	Vacuum
Max. W/m/K	1.20	1.65 (Vac.) 0.95 (Amb.)	1.74	0.86	1.36	0.72
Avg. W/m/K	0.44	0.52 (Vac.) 0.71 (Amb.)	0.83	0.73	0.96	0.53
Min., W/m/K	0.03	0.11 (Vac.) 0.49 (Amb.)	0.56	0.50	0.45	0.40

Table 5 Summary of the calculated thermal inertia of Ryugu samples.

Sample	C0002-p3	C0002-p4	C0025	A0026	C0033	A0064
Pressure	Vacuum	Vacuum & Ambient	Ambient	Ambient	Ambient	Vacuum
Max., $J/s^{1/2}/m^2/K$	1371	1613 (Vac.) 1221 (Amb.)	1641	1103	1510	1085
Avg., $J/s^{1/2}/m^2/K$	791	855 (Vac.) 1052 (Amb.)	1145	1023	1253	926
Min., $J/s^{1/2}/m^2/K$	241	403 (Vac.) 873 (Amb.)	931	845	869	800

6 Conclusion

The thermal diffusivity of the six Ryugu samples from five individual grains; C0002-plate 3, C0002-plate 4, C0025, A0026, C0033, and A0064, were measured by the periodic heating method using lock-in thermography. The measurements showed that there is local thermal anisotropy seemingly caused by cracks inside the sample. The average thermal diffusivity values ranged from 2.8−5.8 × 10^{-7} m^2/s. Samples with a cracked appearance tended to show greater anisotropy in the thermal diffusivity distribution and a greater scattering in the measured values. The thermal diffusivity tended to be larger under atmospheric pressure when comparing the measurement results under atmospheric pressure and vacuum. This is considered to be due to the mitigation of the reduction in heat conduction by the air filled in the cracks or voids. However, anisotropy seems relatively unchanged between the measurements under vacuum and in the air, and the thermal diffusivity of A0064 measured under vacuum was isotropic and showed little scattering. The isotropy of A0064 suggests that micro or nanovoids

on a smaller scale than cracks seen in C0025 and C0033 may be distributed homogeneously in the interior of the Ryugu sample. The thermal conductivity of the Ryugu sample, which was converted from the measured thermal diffusivity, was about 23 % of that of serpentine, which is commonly used to calculate the thermal evolution of carbonaceous asteroids and comets. On the other hand, the converted thermal inertia of the Ryugu sample is about 3.5 times larger than the observed thermal inertia of the asteroid Ryugu's surface, implying that the value of thermal effusivity varies depending on the measurement scale. This difference in thermal inertia between mm- to cm-sized returned samples and boulders could be due to the presence of large-scale cracks caused by meteor impacts and thermal stresses on a scale larger than several hundreds of micrometers in rocks and boulders on Ryugu.

Declarations

Author Contributions

T.I. conceptualization, methodology, investigation, formal analysis, preparing figures, writing—original draft. H.N., conceptualization, resources, writing—review & editing, supervision, funding acquisition. S.T., and S.N. conceptualization, investigation, resources, writing—review & editing. T.N. contributed to organizing the research of the analysis of the properties of Ryugu samples. T.O. contributed to Hayabusa2 mission sample collection; apparatus development. R.F., and A.A. contributed to measurement; analysis. T.M., M.K., K.A., and E.K. contributed to the research of the analysis of the properties of Ryugu samples. H.Y., T.N., R.O., H.Y., H.N., K.S., and S.T. contributed to organizing the research of the analysis of the properties of Ryugu samples. S.W., and Y.T. contributed to Hayabusa2 mission sample collection.

Data Availability

The datasets generated during and analyzed during the current study are available from the corresponding author on reasonable request.

Conflict of interest

The authors declare that they have no known competing financial interests or personal relationships that could have appeared to influence the work reported in this article.

References

1. T. Yokoyama, K. Nagashima, I. Nakai, E. D. Young, Y. Abe, J. Aléon, C. M. O. Alexander, S. Amari, Y. Amelin, K. Bajo, M. Bizzarro, A. Bouvier, R. W. Carlson, M. Chaussidon, B.-G. Choi, N. Dauphas, A. M. Davis, T. di Rocco, W. Fujiya, R. Fukai, I. Gautam, M. K. Haba, Y. Hibiya, H. Hidaka, H. Homma, P. Hoppe, G. R. Huss, K. Ichida, T. Iizuka, T. R. Ireland, A. Ishikawa, M. Ito, S. Itoh, N. Kawasaki, N. T. Kita, K. Kitajima, T. Kleine, S. Komatani, A. N. Krot, M.-C. Liu, Y. Masuda, K. D. McKeegan, M. Morita, K. Motomura, F. Moynier, A. Nguyen, L. Nittler, M. Onose, A. Pack, C. Park, L. Piani, L. Qin, S. S. Russell, N. Sakamoto, M. Schönbächler, L. Tafla, H. Tang, K. Terada, Y. Terada, T. Usui, S. Wada, M. Wadhwa, R. J. Walker, K. Yamashita, Q.-Z. Yin, S. Yoneda, H. Yui, A.-C. Zhang, H. C. Connolly, D. S. Lauretta, T. Nakamura, H. Naraoka, T. Noguchi, R. Okazaki, K. Sakamoto, H. Yabuta, M. Abe, M. Arakawa, A. Fujii, M. Hayakawa, N. Hirata, N. Hirata, R. Honda, C. Honda, S. Hosoda, Y. Iijima, H. Ikeda, M. Ishiguro, Y. Ishihara, T. Iwata, K. Kawahara, S. Kikuchi, K. Kitazato, K. Matsumoto, M. Matsuoka, T. Michikami, Y. Mimasu, A. Miura, T. Morota, S. Nakazawa, N.

Namiki, H. Noda, R. Noguchi, N. Ogawa, K. Ogawa, T. Okada, C. Okamoto, G. Ono, M. Ozaki, T. Saiki, N. Sakatani, H. Sawada, H. Senshu, Y. Shimaki, K. Shirai, S. Sugita, Y. Takei, H. Takeuchi, S. Tanaka, E. Tatsumi, F. Terui, Y. Tsuda, R. Tsukizaki, K. Wada, S. Watanabe, M. Yamada, T. Yamada, Y. Yamamoto, H. Yano, Y. Yokota, K. Yoshihara, M. Yoshikawa, K. Yoshikawa, S. Furuya, K. Hatakeda, T. Hayashi, Y. Hitomi, K. Kumagai, A. Miyazaki, A. Nakato, M. Nishimura, H. Soejima, A. Suzuki, T. Yada, D. Yamamoto, K. Yogata, M. Yoshitake, S. Tachibana, H. Yurimoto, Science (1979), abn7850 (2022)

2. D. J. Tholen, in *Asteroids II*, edited by R. P. Binzel, T. Gehrels, M. Shapley. Matthews (University of Arizona Press, 1989), p. 1139

3. F. E. DeMeo, C. M. O. Alexander, K. J. Walsh, C. R. Chapman, in *Asteroids IV*, edited by P. Michel (University of Arizona Press, 2015), p. 13

4. T. Okada, T. Fukuhara, S. Tanaka, M. Taguchi, T. Arai, H. Senshu, N. Sakatani, Y. Shimaki, H. Demura, Y. Ogawa, K. Suko, T. Sekiguchi, T. Kouyama, J. Takita, T. Matsunaga, T. Imamura, T. Wada, S. Hasegawa, J. Helbert, T. G. Müller, A. Hagermann, J. Biele, M. Grott, M. Hamm, M. Delbo, N. Hirata, N. Hirata, Y. Yamamoto, S. Sugita, N. Namiki, K. Kitazato, M. Arakawa, S. Tachibana, H. Ikeda, M. Ishiguro, K. Wada, C. Honda, R. Honda, Y. Ishihara, K. Matsumoto, M. Matsuoka, T. Michikami, A. Miura, T. Morota, H. Noda, R. Noguchi, K. Ogawa, K. Shirai, E. Tatsumi, H. Yabuta, Y. Yokota, M. Yamada, M. Abe, M. Hayakawa, T. Iwata, M. Ozaki, H. Yano, S. Hosoda, O. Mori, H. Sawada, T. Shimada, H. Takeuchi, R. Tsukizaki, A. Fujii, C. Hirose, S. Kikuchi, Y. Mimasu, N. Ogawa, G. Ono, T. Takahashi, Y. Takei, T. Yamaguchi, K. Yoshikawa, F. Terui, T. Saiki, S. Nakazawa, M. Yoshikawa, S. Watanabe, Y. Tsuda, Nature **579**, 518 (2020)

5. E. Nakamura, K. Kobayashi, R. Tanaka, T. Kunihiro, H. Kitagawa, C. Potiszil, T. Ota, C. Sakaguchi, M. Yamanaka, D. M. Ratnayake, H. Tripathi, R. Kumar, M.-L. Avramescu, H. Tsuchida, Y. Yachi, H. Miura, M. Abe, R. Fukai, S. Furuya, K. Hatakeda, T. Hayashi, Y. Hitomi, K. Kumagai, A. Miyazaki, A. Nakato, M. Nishimura, T. Okada, H. Soejima, S. Sugita, A. Suzuki, T. Usui, T. Yada, D. Yamamoto, K. Yogata, M. Yoshitake, M. Arakawa, A. Fujii, M. Hayakawa, N. Hirata, N. Hirata, R. Honda, C. Honda, S. Hosoda, Y. Iijima, H. Ikeda, M. Ishiguro, Y. Ishihara, T. Iwata, K. Kawahara, S. Kikuchi, K. Kitazato, K. Matsumoto, M. Matsuoka, T. Michikami, Y. Mimasu, A. Miura, T. Morota, S. Nakazawa, N. Namiki, H. Noda, R. Noguchi, N. Ogawa, K. Ogawa, C. Okamoto, G. Ono, M. Ozaki, T. Saiki, N. Sakatani, H. Sawada, H. Senshu, Y. Shimaki, K. Shirai, Y. Takei, H. Takeuchi, S. Tanaka, E. Tatsumi, F. Terui, R. Tsukizaki, K. Wada, M. Yamada, T. Yamada, Y. Yamamoto, H. Yano, Y. Yokota, K. Yoshihara, M. Yoshikawa, K. Yoshikawa, M. Fujimoto, S. Watanabe, Y. Tsuda, Proc. Jpn. Acad., Series B **98**, 227 (2022)

6. S. Sugita, R. Honda, T. Morota, S. Kameda, H. Sawada, E. Tatsumi, M. Yamada, C. Honda, Y. Yokota, T. Kouyama, N. Sakatani, K. Ogawa, H. Suzuki, T. Okada, N. Namiki, S. Tanaka, Y. Iijima, K. Yoshioka, M. Hayakawa, Y. Cho, M. Matsuoka, N. Hirata, N. Hirata, H. Miyamoto, D. Domingue, M. Hirabayashi, T. Nakamura, T. Hiroi, T. Michikami, P. Michel, R. L. Ballouz, O. S. Barnouin, C. M. Ernst, S. E. Schröder, H. Kikuchi, R. Hemmi, G. Komatsu, T. Fukuhara, M. Taguchi, T. Arai, H. Senshu, H. Demura, Y. Ogawa, Y. Shimaki, T. Sekiguchi, T. G. Müller, A. Hagermann, T. Mizuno, H. Noda, K. Matsumoto, R. Yamada, Y. Ishihara, H. Ikeda, H. Araki, K. Yamamoto, S. Abe, F. Yoshida, A. Higuchi, S. Sasaki, S. Oshigami, S. Tsuruta, K. Asari, S. Tazawa, M. Shizugami, J. Kimura, T. Otsubo, H. Yabuta, S. Hasegawa, M. Ishiguro, S. Tachibana, E. Palmer, R. Gaskell, L. le Corre, R. Jaumann, K. Otto, N. Schmitz, P. A. Abell, M. A. Barucci, M. E. Zolensky, F. Vilas, F. Thuillet, C. Sugimoto, N. Takaki, Y. Suzuki, H. Kamiyoshihara, M. Okada, K. Nagata, M. Fujimoto, M. Yoshikawa, Y. Yamamoto, K. Shirai, R. Noguchi, N. Ogawa, F. Terui, S. Kikuchi, T. Yamaguchi, Y. Oki, Y. Takao, H.

Takeuchi, G. Ono, Y. Mimasu, K. Yoshikawa, T. Takahashi, Y. Takei, A. Fujii, C. Hirose, S. Nakazawa, S. Hosoda, O. Mori, T. Shimada, S. Soldini, T. Iwata, M. Abe, H. Yano, R. Tsukizaki, M. Ozaki, K. Nishiyama, T. Saiki, S. Watanabe, Y. Tsuda, Science (1979) **364**, (2019)

7. E. Tatsumi, N. Sakatani, L. Riu, M. Matsuoka, R. Honda, T. Morota, S. Kameda, T. Nakamura, M. Zolensky, R. Brunetto, T. Hiroi, S. Sasaki, S. Watanabe, S. Tanaka, J. Takita, C. Pilorget, J. de León, M. Popescu, J. L. Rizos, J. Licandro, E. Palomba, D. Domingue, F. Vilas, H. Campins, Y. Cho, K. Yoshioka, H. Sawada, Y. Yokota, M. Hayakawa, M. Yamada, T. Kouyama, H. Suzuki, C. Honda, K. Ogawa, K. Kitazato, N. Hirata, N. Hirata, Y. Tsuda, M. Yoshikawa, T. Saiki, F. Terui, S. Nakazawa, Y. Takei, H. Takeuchi, Y. Yamamoto, T. Okada, Y. Shimaki, K. Shirai, S. Sugita, Nature Communications 2021 12:1 **12**, 1 (2021)

8. H. Campins, J. de León, A. Morbidelli, J. Licandro, J. Gayon-Markt, M. Delbo, P. Michel, Astron. J. **146**, 26 (2013)

9. K. J. Walsh, M. Delbó, W. F. Bottke, D. Vokrouhlický, D. S. Lauretta, Icarus **225**, 283 (2013)

10. C. P. Opeil, G. J. Consolmagno, D. T. Britt, Icarus **208**, 449 (2010)

11. G. J. Consolmagno, Thermal History Models of Icy Satellites, Master Thesis, Massachusetts Institute of Technology, (1975)

12. B. A. Cohen, R. F. Coker, Icarus **145**, 369 (2000)

13. R. J. Macke, G. J. Consolmagno, D. T. Britt, Meteorit. Planet. Sci. **46**, 1842 (2011)

14. D. Ostrowski, K. Bryson, Planet. Space Sci. **165**, 148 (2019)

15. T. Ishizaki, T. Kawahara, K. Tomioka, S. Tanaka, N. Sakatani, T. Nakamura, H. Nagano, Int. J. Thermophys. **43**, 97 (2022)

16. C. P. Opeil, G. J. Consolmagno, D. J. Safarik, D. T. Britt, Meteorit. Planet. Sci. **47**, 319 (2012)

17. T. Nakamura, M. Matsumoto, K. Amano, Y. Enokido, M. E. Zolensky, T. Mikouchi, H. Genda, S. Tanaka, M. Y. Zolotov, K. Kurosawa, S. Wakita, R. Hyodo, H. Nagano, D. Nakashima, Y. Takahashi, Y. Fujioka, M. Kikuiri, E. Kagawa, M. Matsuoka, A. J. Brearley, A. Tsuchiyama, M. Uesugi, J. Matsuno, Y. Kimura, M. Sato, R. E. Milliken, E. Tatsumi, S. Sugita, T. Hiroi, K. Kitazato, D. Brownlee, D. J. Joswiak, M. Takahashi, K. Ninomiya, T. Takahashi, T. Osawa, K. Terada, F. E. Brenker, B. J. Tkalcec, L. Vincze, R. Brunetto, A. Aléon-Toppani, Q. H. S. Chan, M. Roskosz, J.-C. Viennet, P. Beck, E. E. Alp, T. Michikami, Y. Nagaashi, T. Tsuji, Y. Ino, J. Martinez, J. Han, A. Dolocan, R. J. Bodnar, M. Tanaka, H. Yoshida, K. Sugiyama, A. J. King, K. Fukushi, H. Suga, S. Yamashita, T. Kawai, K. Inoue, A. Nakato, T. Noguchi, F. Vilas, A. R. Hendrix, C. Jaramillo-Correa, D. L. Domingue, G. Dominguez, Z. Gainsforth, C. Engrand, J. Duprat, S. S. Russell, E. Bonato, C. Ma, T. Kawamoto, T. Wada, S. Watanabe, R. Endo, S. Enju, L. Riu, S. Rubino, P. Tack, S. Takeshita, Y. Takeichi, A. Takeuchi, A. Takigawa, D. Takir, T. Tanigaki, A. Taniguchi, K. Tsukamoto, T. Yagi, S. Yamada, K. Yamamoto, Y. Yamashita, M. Yasutake, K. Uesugi, I. Umegaki, I. Chiu, T. Ishizaki, S. Okumura, E. Palomba, C. Pilorget, S. M. Potin, A. Alasli, S. Anada, Y. Araki, N. Sakatani, C. Schultz, O. Sekizawa, S. D. Sitzman, K. Sugiura, M. Sun, E. Dartois, E. de Pauw, Z. Dionnet, Z. Djouadi, G. Falkenberg, R. Fujita, T. Fukuma, I. R. Gearba, K. Hagiya, M. Y. Hu, T. Kato, T. Kawamura, M. Kimura, M. K. Kubo, F. Langenhorst, C. Lantz, B. Lavina, M. Lindner, J. Zhao, B. Vekemans, D. Baklouti, B. Bazi, F. Borondics, S. Nagasawa, G. Nishiyama, K. Nitta, J. Mathurin, T. Matsumoto, I. Mitsukawa, H. Miura, A. Miyake, Y. Miyake, H. Yurimoto, R. Okazaki, H. Yabuta, H. Naraoka, K. Sakamoto, S. Tachibana, H. C. Connolly, D. S. Lauretta, M. Yoshitake, M. Yoshikawa, K. Yoshikawa, K. Yoshihara, Y. Yokota, K. Yogata, H. Yano, Y. Yamamoto, D. Yamamoto, M. Yamada, T. Yamada, T. Yada, K. Wada, T. Usui, R. Tsukizaki, F. Terui, H. Takeuchi, Y. Takei, A. Iwamae,

H. Soejima, K. Shirai, Y. Shimaki, H. Senshu, H. Sawada, T. Saiki, M. Ozaki, G. Ono, T. Okada, N. Ogawa, K. Ogawa, R. Noguchi, H. Noda, M. Nishimura, N. Namiki, S. Nakazawa, T. Morota, A. Miyazaki, A. Miura, Y. Mimasu, K. Matsumoto, K. Kumagai, T. Kouyama, S. Kikuchi, K. Kawahara, S. Kameda, T. Iwata, Y. Ishihara, M. Ishiguro, H. Ikeda, S. Hosoda, R. Honda, C. Honda, Y. Hitomi, N. Hirata, N. Hirata, T. Hayashi, M. Hayakawa, K. Hatakeda, S. Furuya, R. Fukai, A. Fujii, Y. Cho, M. Arakawa, M. Abe, S. Watanabe, Y. Tsuda, Science (1979), abn8671 (2022)

18. H. S. Carslaw, J. J. C. Jaeger, Conduction of Heat in Solids, 2nd edn. (Oxford science publications, Oxford science publications, 1959), p. 263

19. T. Ishizaki, H. Nagano, Infrared Phys. Technol. **99**, 248 (2019)

20. T. Ishizaki, H. Nagano, Int. J. Thermophys. **36**, 2577 (2015)

21. A. Mendioroz, R. Fuente-Dacal, E. Apiañiz, and A. Salazar, Rev. Sci. Instrum. **80**, 1 (2009)

22. S. Tachibana, H. Sawada, R. Okazaki, Y. Takano, K. Sakamoto, Y. N. Miura, C. Okamoto, H. Yano, S. Yamanouchi, P. Michel, Y. Zhang, S. Schwartz, F. Thuillet, H. Yurimoto, T. Nakamura, T. Noguchi, H. Yabuta, H. Naraoka, A. Tsuchiyama, N. Imae, K. Kurosawa, A. M. Nakamura, K. Ogawa, S. Sugita, T. Morota, R. Honda, S. Kameda, E. Tatsumi, Y. Cho, K. Yoshioka, Y. Yokota, M. Hayakawa, M. Matsuoka, N. Sakatani, M. Yamada, T. Kouyama, H. Suzuki, C. Honda, T. Yoshimitsu, T. Kubota, H. Demura, T. Yada, M. Nishimura, K. Yogata, A. Nakato, M. Yoshitake, A. I. Suzuki, S. Furuya, K. Hatakeda, A. Miyazaki, K. Kumagai, T. Okada, M. Abe, T. Usui, T. R. Ireland, M. Fujimoto, T. Yamada, M. Arakawa, H. C. Connolly, A. Fujii, S. Hasegawa, N. Hirata, N. Hirata, C. Hirose, S. Hosoda, Y. Iijima, H. Ikeda, M. Ishiguro, Y. Ishihara, T. Iwata, S. Kikuchi, K. Kitazato, D. S. Lauretta, G. Libourel, B. Marty, K. Matsumoto, T. Michikami, Y. Mimasu, A. Miura, O. Mori, K. Nakamura-Messenger, N. Namiki, A. N. Nguyen, L. R. Nittler, H. Noda, R. Noguchi, N. Ogawa, G. Ono, M. Ozaki, H. Senshu, T. Shimada, Y. Shimaki, K. Shirai, S. Soldini, T. Takahashi, Y. Takei, H. Takeuchi, R. Tsukizaki, K. Wada, Y. Yamamoto, K. Yoshikawa, K. Yumoto, M. E. Zolensky, S. Nakazawa, F. Terui, S. Tanaka, T. Saiki, M. Yoshikawa, S. Watanabe, and Y. Tsuda, Science (1979) **375**, 1011 (2022)

23. T. Morota, S. Sugita, Y. Cho, M. Kanamaru, E. Tatsumi, N. Sakatani, R. Honda, N. Hirata, H. Kikuchi, M. Yamada, Y. Yokota, S. Kameda, M. Matsuoka, H. Sawada, C. Honda, T. Kouyama, K. Ogawa, H. Suzuki, K. Yoshioka, M. Hayakawa, N. Hirata, M. Hirabayashi, H. Miyamoto, T. Michikami, T. Hiroi, R. Hemmi, O. S. Barnouin, C. M. Ernst, K. Kitazato, T. Nakamura, L. Riu, H. Senshu, H. Kobayashi, S. Sasaki, G. Komatsu, N. Tanabe, Y. Fujii, T. Irie, M. Suemitsu, N. Takaki, C. Sugimoto, K. Yumoto, M. Ishida, H. Kato, K. Moroi, D. Domingue, P. Michel, C. Pilorget, T. Iwata, M. Abe, M. Ohtake, Y. Nakauchi, K. Tsumura, H. Yabuta, Y. Ishihara, R. Noguchi, K. Matsumoto, A. Miura, N. Namiki, S. Tachibana, M. Arakawa, H. Ikeda, K. Wada, T. Mizuno, C. Hirose, S. Hosoda, O. Mori, T. Shimada, S. Soldini, R. Tsukizaki, H. Yano, M. Ozaki, H. Takeuchi, Y. Yamamoto, T. Okada, Y. Shimaki, K. Shirai, Y. Iijima, H. Noda, S. Kikuchi, T. Yamaguchi, N. Ogawa, G. Ono, Y. Mimasu, K. Yoshikawa, T. Takahashi, Y. Takei, A. Fujii, S. Nakazawa, F. Terui, S. Tanaka, M. Yoshikawa, T. Saiki, S. Watanabe, and Y. Tsuda, Science (1979) **368**, 654 (2020)

24. Y. Shimaki, H. Senshu, N. Sakatani, T. Okada, T. Fukuhara, S. Tanaka, M. Taguchi, T. Arai, H. Demura, Y. Ogawa, K. Suko, T. Sekiguchi, T. Kouyama, S. Hasegawa, J. Takita, T. Matsunaga, T. Imamura, T. Wada, K. Kitazato, N. Hirata, N. Hirata, R. Noguchi, S. Sugita, S. Kikuchi, T. Yamaguchi, N. Ogawa, G. Ono, Y. Mimasu, K. Yoshikawa, T. Takahashi, Y. Takei, A. Fujii, H. Takeuchi, Y. Yamamoto, M. Yamada, K. Shirai, Y. ichi Iijima, K. Ogawa, S. Nakazawa, F. Terui, T. Saiki, M. Yoshikawa, Y. Tsuda, S. ichiro Watanabe, Icarus **348**, 113835 (2020)

Appendix

Figure 11−Figure 17 show the thermal diffusivity distribution and experimental plots of phase lag vs radial distance with a linear approximation line used in thermal diffusivity analysis at the angles of 0 and 90 degree as representative angles. When analyzing the slope of the phase lag with respect to the radial distance, the range of phase lag used in the analysis in each direction was fixed to be constant to eliminate arbitrariness in the selection of the analysis region and to maintain the same quality of the scattering of the results. The upper and lower limits of the phase lag range used in the analysis are indicated by the red plots in figures (b, c). The slope is calculated by a linear approximation for the phase lag in this range. The linear approximation line of the A0026 sample shown in Figure 15 does not seem to fit to the whole experimental plots, this is due to the following. Figure 15 (b) and (c) show that the change of the phase lag decreases around the distance of 0.2−0.4 mm, and this is possibly due to the effect of the reflected temperature wave at the sample edge (0 deg.) or on the back surface on the sample (90 deg.). The fitting analysis was, therefore, performed for the phase lag plots only in the region closer to the heating point.

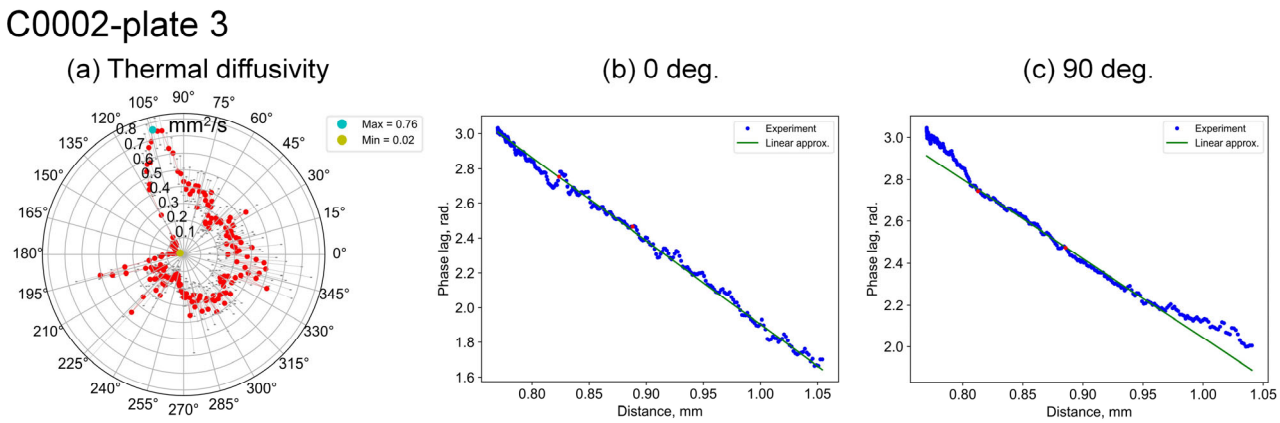

Figure 11 (a) thermal diffusivity distribution of the C0002-plate 3 sample and experimental plots of phase lag vs distance and a linear approximation line used to obtain the thermal diffusivity at the angle of (b) 0 degree and (c) 90 degree.

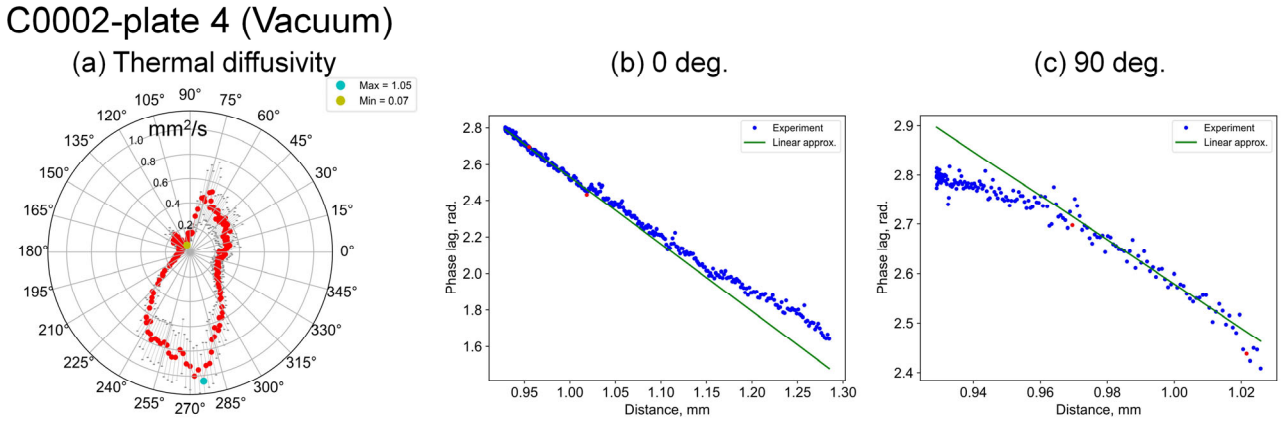

Figure 12 (a) thermal diffusivity distribution of the C0002-plate 4 sample measured under vacuum pressure and experimental plots of phase lag vs distance and a linear approximation line used to obtain the thermal diffusivity at the

angle of (b) 0 degree and (c) 90 degree.

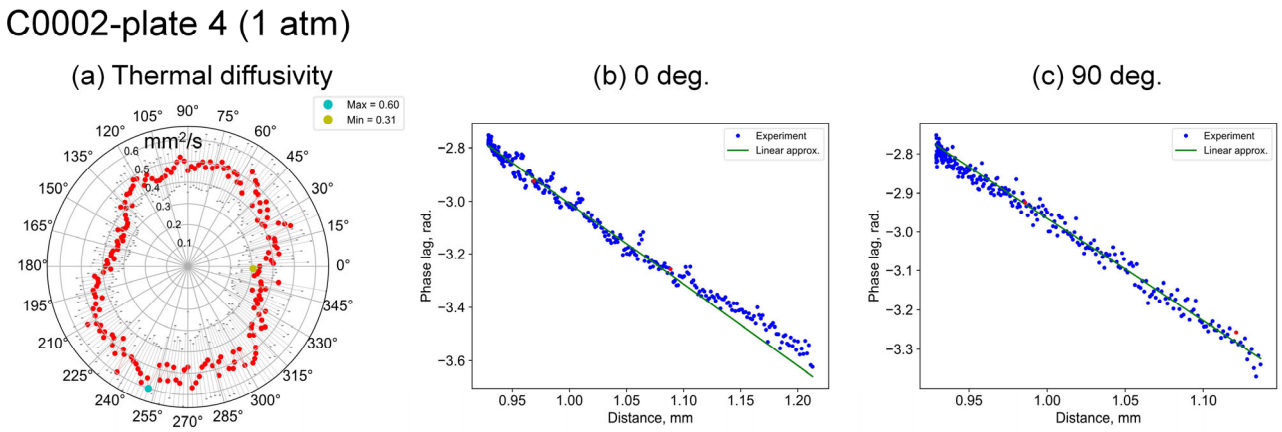

Figure 13 (a) thermal diffusivity distribution of the C0002-plate 4 sample measured under atmospheric pressure and experimental plots of phase lag vs distance and a linear approximation line used to obtain the thermal diffusivity at the angle of (b) 0 degree and (c) 90 degree.

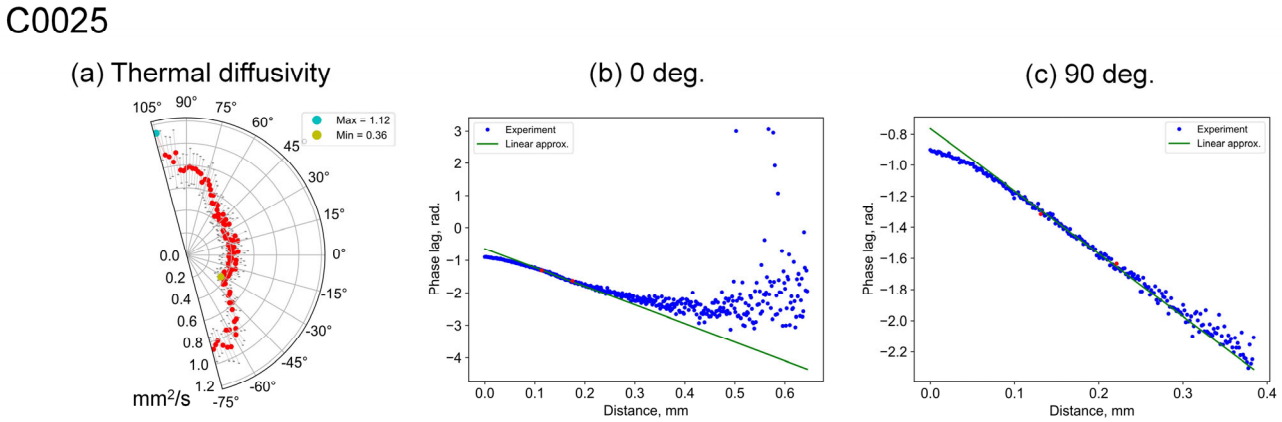

Figure 14 (a) thermal diffusivity distribution of the C0025 sample and experimental plots of phase lag vs distance and a linear approximation line used to obtain the thermal diffusivity at the angle of (b) 0 degree and (c) 90 degree.

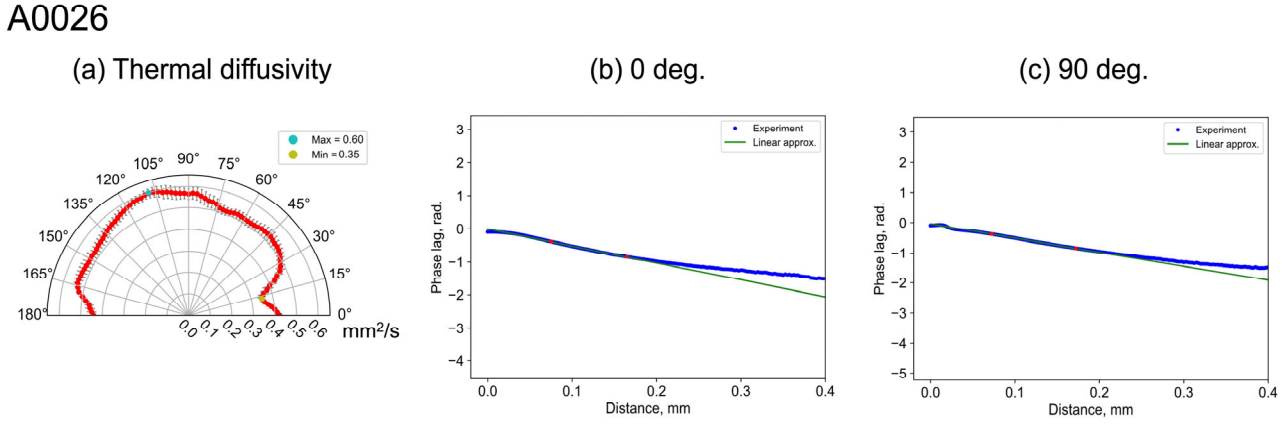

Figure 15 (a) thermal diffusivity distribution of the A0026 sample and experimental plots of phase lag vs distance and a linear approximation line used to obtain the thermal diffusivity at the angle of (b) 0 degree and (c) 90 degree.

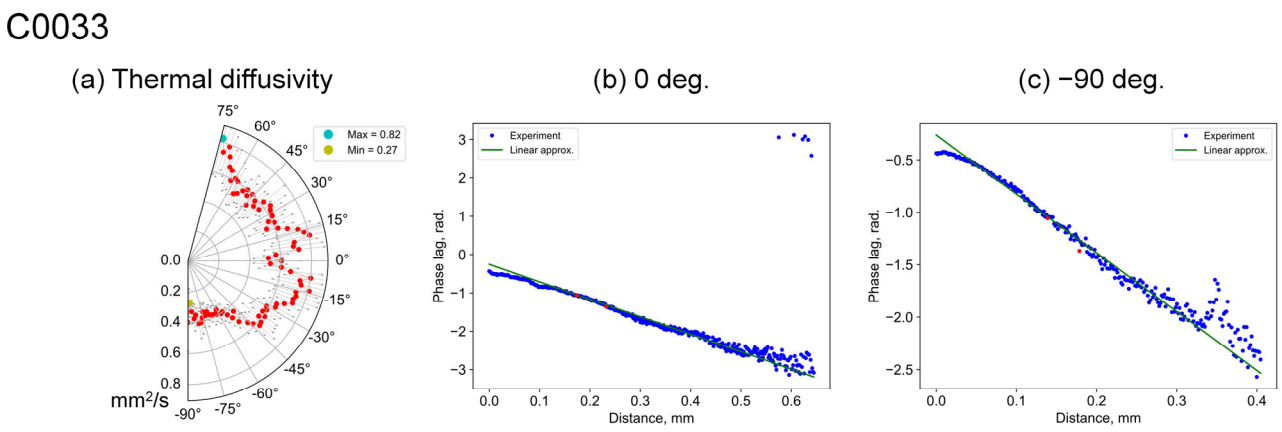

Figure 16 (a) thermal diffusivity distribution of the C0033 sample and experimental plots of phase lag vs distance and a linear approximation line used to obtain the thermal diffusivity at the angle of (b) 0 degree and (c) 90 degree.

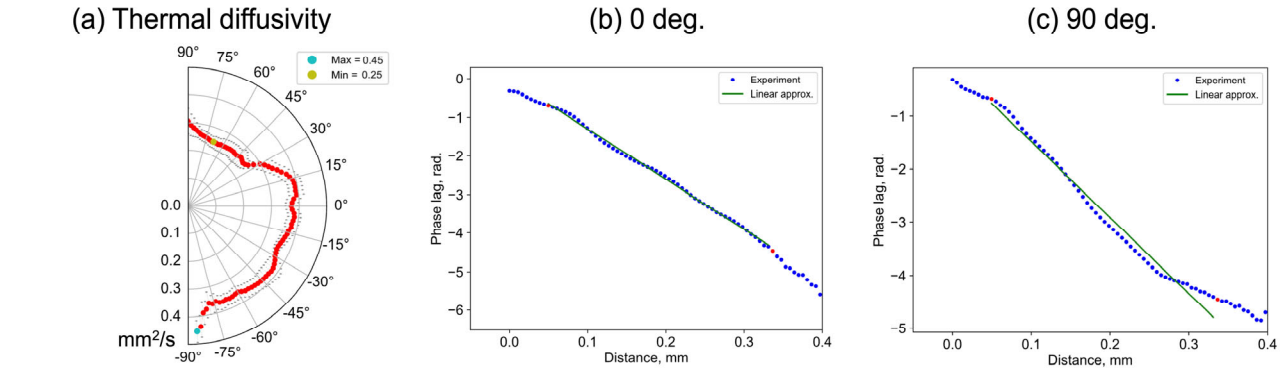

Figure 17 (a) thermal diffusivity distribution of the C0002-plate 3 sample and experimental plots of phase lag vs distance and a linear approximation line used to obtain the thermal diffusivity at the angle of (b) 0 degree and (c) 90 degree.